

# Heterogeneous Oxidation Reaction of Gas-Phase Ozone with Anthracene in Thin Films and on Aerosols by Infrared Spectroscopic Methods

JUAN J. NÁJERA,<sup>1</sup> RUTH WAMSLEY,<sup>1</sup> DEBORAH J. LAST,<sup>2</sup> KIMBERLEY E. LEATHER,<sup>1</sup> CARL J. PERCIVAL,<sup>1</sup> ANDREW B. HORN<sup>2</sup>

<sup>1</sup>*School of Earth, Atmospheric and Environmental Sciences, Faculty of Engineering and Physical Sciences, The University of Manchester, Manchester M13 9PL, UK*

<sup>2</sup>*School of Chemistry, Faculty of Engineering and Physical Sciences, The University of Manchester, Manchester M13 9PL, UK*

*Received 23 January 2011; revised 21 May 2011; accepted 23 May 2011*

*DOI 10.1002/kin.20602*

*Published online 14 September 2011 in Wiley Online Library (wileyonlinelibrary.com).*

**ABSTRACT:** In this paper, a real-time laboratory study of the heterogeneous oxidation reaction of gas-phase ozone with anthracene on surface substrates by using infrared spectroscopy in two distinctly different experimental configurations is reported. One set of kinetic measurements was made by attenuated total internal reflection infrared (ATR-IR) spectroscopy using approximately 75-nm films of anthracene adsorbed on ZnSe, for which the reactive uptake coefficient was determined to be  $(2.0 \pm 1.1) \times 10^{-7}$ . Using an aerosol flow tube coupled to an infrared spectrometer (AFT-IR), similar measurements were made on  $(\text{NH}_4)_2\text{SO}_4$  (ammonium sulfate) aerosols coated with a 0.1- $\mu\text{m}$  film of anthracene. The aerosol kinetic results as a function of the ozone concentration are consistent with a Langmuir–Hinshelwood-type mechanism, for which the ozone-partitioning coefficient was  $K_{\text{O}_3} = (1.4 \pm 1.7) \times 10^{-16} \text{ cm}^3 \text{ molecule}^{-1}$ , and the maximum pseudo-first-order rate coefficient was  $k_{\text{max}}^1 = (0.035 \pm 0.016) \text{ s}^{-1}$ . Infrared spectroscopic and mass spectrometric analysis of the ozonolysis reaction in the bulk phase identified the main ozonolysis products as dihydroxyanthrones, 9,10-endoperoxide–anthracene, 9,10-anthraquinone, and anthrone. Larger products were also seen in the mass spectra, most likely the result of secondary product and oligomer formation. © 2011 Wiley Periodicals, Inc. *Int J Chem Kinet* 43: 694–707, 2011

## INTRODUCTION

Polycyclic aromatic hydrocarbons (PAHs) are released during incomplete combustion processes and have

*Correspondence to:* Carl J. Percival; e-mail: carl.percival@manchester.ac.uk  
© 2011 Wiley Periodicals, Inc.

been identified as an important class of pollutants that are ubiquitous in the atmosphere [1]. PAHs are known to be carcinogenic, mutagenic, and allergenic in nature [2]. After emission, the atmospheric processing of PAHs in the gas- and condensed-phase defines their environmental fate [3]. The most significant transformation pathway is the heterogeneous reaction with atmospheric oxidants such as OH and NO<sub>3</sub> radicals and ozone. These reactions result in the formation of oxidized polycyclic aromatic hydrocarbons (OPAHs), which are often more toxic than the parent PAHs [4]. OPAHs such as quinones can also be emitted directly into the atmosphere from combustion sources. The potential for PAHs and OPAHs to affect human health through direct inhalation has fuelled interest in the oxidation reactions of these compounds because their atmospheric chemistry is far from well understood [1]. A number of recent experimental studies have utilized anthracene as a PAH proxy representative of the wider class of aromatic species because it is present in polluted atmospheres at typical concentrations [1] of approximately 6 ng m<sup>-3</sup>. Early studies of the liquid-phase reaction of anthracene solution with dissolved ozone by Bailey [5] identified 9,10-anthraquinone and phthalic acid as the main reaction products. From these studies, a reaction mechanism was postulated, where 9,10-anthraquinone was formed either directly by consecutive ozone attack of the carbons on the inner ring of anthracene or produced indirectly by reduction of the hydroperoxide intermediate during workup [5]. More recent studies have concentrated on characterizing the ozonolysis mechanism and product yields for anthracene on a variety of different substrates such as aqueous and organic interfaces [3,6,7], film surfaces [8], and on both organic and inorganic aerosol surfaces [2,9]. There are, however, significant discrepancies in both the experimentally reported reaction products and the reported rates of reaction for ozonolysis.

In this study, real-time infrared spectroscopic studies of the oxidation reactions of anthracene by ozone as a thin film and in the aerosol phase are reported, supported by a qualitative product study in bulk solution using both infrared spectroscopy and mass spectrometry.

## EXPERIMENTAL

### Bulk Solution Phase

Solutions were prepared in ethyl acetate at typical solute concentrations of 10 mM. The ozonolysis reaction was carried out in a 5-mL reaction vessel [10], through which ozone was bubbled at a controlled rate. A 20-sccm flow of O<sub>2</sub> was passed through a voltage

discharge ozone generator to produce an ozone concentration of  $2.4 \times 10^4$  ppm. The reaction time was varied between 0.5 and 8 min. The gas bleed was introduced via a medium-gauge needle and exhausted through a second needle. Infrared spectra were recorded using a commercial diamond attenuated total internal reflection (ATR) attachment (Pike Miracle; Pike Technologies, Madison, WI) fitted inside the sample compartment of a Fourier transform infrared spectroscopy (FTIR) spectrometer (JASCO model 2400; JASCO, Great Dunmow, UK). A micropipetted amount (1 or 2  $\mu$ L) of the sample solution was deposited, and the solvent (ethyl acetate) was allowed to evaporate prior to spectra being recorded. Data were recorded for a pure anthracene solution as well as for samples at various stages of the ozonolysis reaction. A total of 128 spectra were collected at a resolution of 4 cm<sup>-1</sup> and coadded to create an absorbance spectrum.

Samples were also analyzed by atmospheric pressure chemical ionization (APCI) mass spectrometry using a service instrument at the University of Manchester. Both positive and negative ionization spectra were recorded. The carrier gas used was nitrogen, and the sample was volatilized instantly at 450–550°C close to the probe.

### ATR-IR Spectroscopy of Reactions in Thin Films

Thin-film studies were performed using an attenuated total internal reflection infrared (ATR-IR) spectroscopic method that has been described in detail elsewhere [11]. Briefly, the film study was performed on a ZnSe internal reflection element (IRE) (Spectral Systems LLC, New York, NY) mounted on a custom-built ATR accessory in a Thermo-Nicolet FTIR Nexus spectrometer (ThermoFisher Scientific, Inc., Waltham, MA). The thin films were formed on the IRE via a method known as casting, whereby a solution of anthracene was spread over the crystal, and the solvent was allowed to evaporate. A 30- $\mu$ L aliquot of a 10-mM solution of anthracene in ethyl acetate was placed on the crystal. The film produced allowed for an exact volume of anthracene to be determined with highly repeatable spectroscopic characteristics. Once the films were cast, ozone was flowed over the film with spectra collected every minute and recorded as the sum of 64 scans at 4 cm<sup>-1</sup> resolution. The ozone concentration was determined by measuring the absorption at 254 nm ( $\sigma = 1.15 \times 10^{-17}$  cm<sup>3</sup> molecules<sup>-1</sup>) [12] in a laboratory-built gas cell in a Perkin-Elmer (Waltham, MA) Lambda 25 UV-vis spectrometer. The concentration of ozone used in the thin-film kinetic experiment was 2 ppm.

## Aerosol Flow Tube Studies

The aerosol flow tube (AFT) system and the FTIR spectrometer detection system used in this work have been described elsewhere [11,13]. Briefly an overview of the technique will be given here with an emphasis on the experimental conditions and procedures specific to this kinetic study. To generate the anthracene particles, a seed particle of ammonium sulfate ( $(\text{NH}_4)_2\text{SO}_4$ ) was required, which was coated with anthracene vapor. The particle size distributions were then measured using a commercial-process aerosol monitor (PAM 510; TOPAS GmbH) before entering the flow tube. Aerosol particle dimensions were described by lognormal distributions with standard deviation  $\sigma < 1.15$ , where their average particle diameter ( $D_p$ ) and the number of particles ( $N'$ ) were obtained [13]. The coated particles were diluted after entering the AFT by a sheath flow. The main AFT reactor consists of a 100-cm long, vertically orientated Pyrex glass flow tube with an internal diameter of 4.0 cm. A movable stainless steel injector, 146.5 cm long and having an internal diameter of 1.0 cm, was inserted axially down the center of the flow tube, through which a variable oxygen/nitrogen flow mixture was injected. In the kinetic experiments, a total flow of 1160 sccm was used which resulted in an average linear flow velocity of  $\sim 1.4 \text{ cm s}^{-1}$  and a Reynolds number of  $\sim 36$ . The contact time was varied by setting the movable injector to different positions from 15 to 80 cm along the length of the flow tube, which was equivalent to a contact time of 11–57 s.

The infrared detection system used in the kinetic aerosol experiments has been described in detail elsewhere [11]. In these experiments, the multipass long path cell was based on a white cell configuration, which operated at 16 passes, or  $47.0 \pm 0.9 \text{ cm}$  pathlength and was mounted perpendicular to the direction of the flow. The aerosol flow crosses the infrared detection perpendicular to the multipass optics immediately prior to exiting the flow tube. Infrared spectra were acquired in situ using a modified commercial FTIR spectrometer (Nexus; Thermo Nicolet), and the spectra were measured at a resolution of  $4 \text{ cm}^{-1}$  from the coaddition of 256 scans. In this study, experiments were performed at room temperature (298 K), atmospheric pressure (1 atm), and at varying ozone concentrations.

The concentration of ozone present in the AFT experiments was determined from three characteristic bands that were observed in the infrared spectrum of ozone: the peak height of the absorption band at  $2123 \text{ cm}^{-1}$ , the peak area  $2138\text{--}2046 \text{ cm}^{-1}$  (using a baseline  $2150\text{--}2040 \text{ cm}^{-1}$  for both), and area band  $1072\text{--}991 \text{ cm}^{-1}$  (using a baseline  $1080\text{--}970 \text{ cm}^{-1}$ ).

The average ozone concentration obtained from the analysis of these bands determined the ozone concentration in the AFT within 5% error. The concentrations determined from the infrared bands were validated by a cross calibration using a laboratory-built gas cell in a Perkin–Elmer Lambda 25 UV–vis spectrometer. In the aerosol kinetic experiments, the ozone concentration was varied between 150 and 750 ppm with an uncertainty of approximately 5%.

## Chemicals

All chemicals were purchased from Sigma Aldrich Co., Ltd. (Dorset, UK), and used without further purification: anthracene (99%), 9,10-anthraquinone (97%), ethyl acetate (analytical reagent 99.98% assay), and  $(\text{NH}_4)_2\text{SO}_4$  (99.98%). Ozone was generated by passing a flow of pure oxygen (BOC Gases, Guilford, UK) through either a commercial ozone generator (BMT802; BMT Messtechnik GmbH, Berlin, Germany) for both the solution and aerosol experiments or by irradiation at 185 nm in an ozone generator with variable UV lamp exposure (UVP LLC, Upland, CA) for thin-film experiments. The carrier gas used in all experiments was dry nitrogen (BOC Gases).

## RESULTS AND DISCUSSION

### Solution Studies of Anthracene Ozonolysis

**Infrared Spectroscopy.** The infrared spectra for pure anthracene and at various stages of ozonolysis are shown in Fig. 1a, and the main absorption bands for pure anthracene are presented in Table I. For unreacted anthracene, the majority of the main bands are associated with the vibrational modes of the conjugated aromatic rings [14]. The principal characteristic features are the C–H stretching modes in the region  $3070\text{--}2960 \text{ cm}^{-1}$ , the overtones and combination modes between  $1930$  and  $1720 \text{ cm}^{-1}$ , the skeletal C=C vibrations between  $1620$  and  $1445 \text{ cm}^{-1}$ , the C–H in plane (ip) vibrations between  $1315$  and  $1145 \text{ cm}^{-1}$ , and the out of plane (oop) C–H bending modes below  $885 \text{ cm}^{-1}$ . The latter are the most intense bands in the ATR-IR spectrum and are seen at  $883$  and  $725 \text{ cm}^{-1}$  [15].

Upon ozone exposure, a number of spectral changes are apparent as a reaction occurs, as shown in Figs. 1b–1g. The characteristic bands of anthracene decrease in intensity to be replaced by a large number of new features. In particular, the sharp aromatic  $\nu$  (C–H) bands

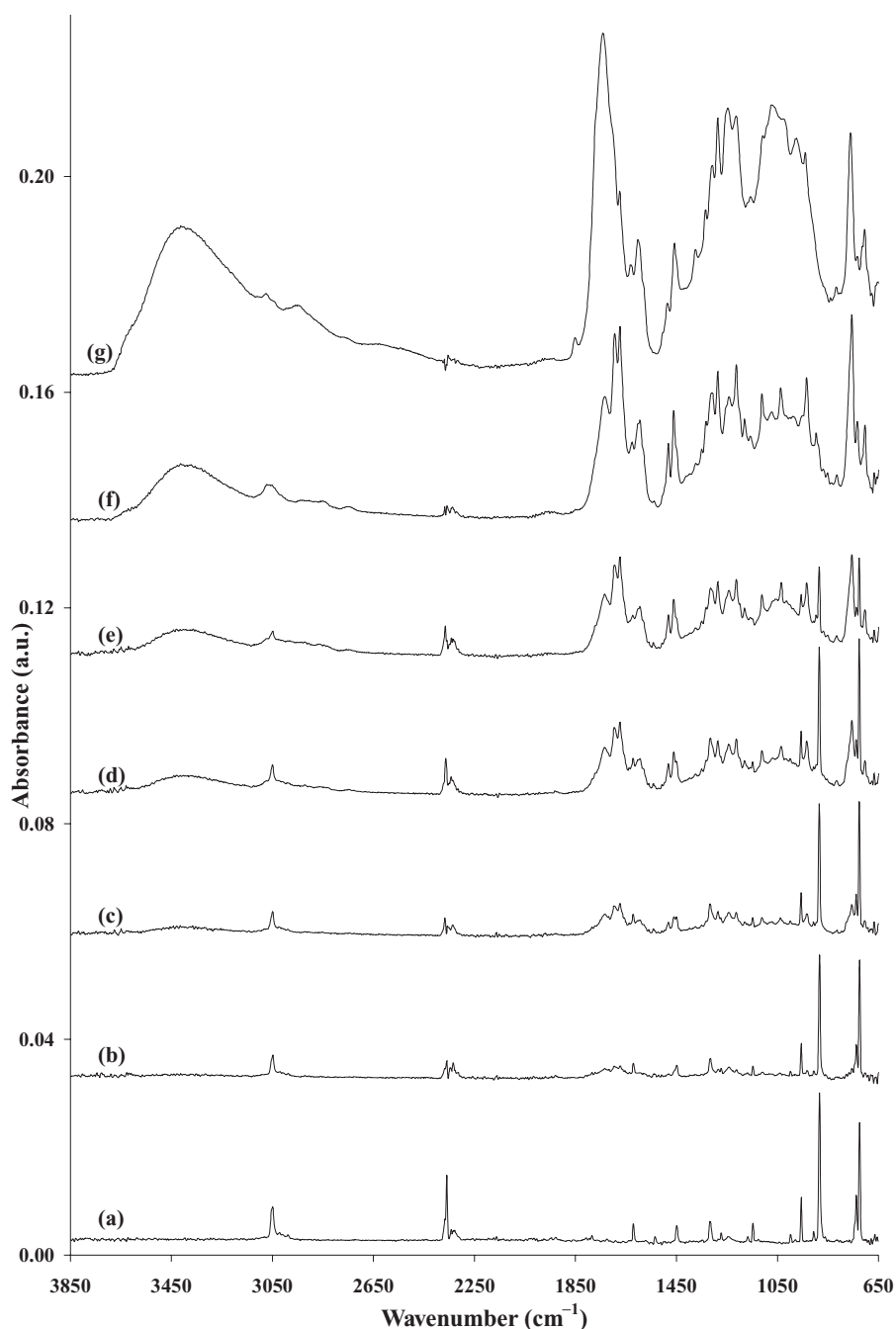


**Figure 1** ATR-IR spectra of anthracene ozonized in ethyl acetate solution for (a) 0 min, (b) 1 min, (c) 1.5 min, (d) 2 min, (e) 3 min, (f) 4 min, and (g) 8 min.

in the region  $3070\text{--}2960\text{ cm}^{-1}$  are lost during the reaction with ozone and are replaced by broad, unstructured bands in roughly the same region. As the new features are still above ca.  $3000\text{ cm}^{-1}$ , it seems likely that the new species formed are also substantially aromatic in nature. A similar decrease in intensity can be seen for the anthracene-specific out-of-plane  $\delta$  (C–H)

modes in the region  $885\text{--}700\text{ cm}^{-1}$ , although these are also replaced by strong, broad spectral features in roughly the same region. Because the anthracene-specific bands at  $3050$  and  $883\text{ cm}^{-1}$  are characteristically sharp and in relatively clear spectral regions, these bands can be used for the determination of reactant loss kinetics.

**Table I** Summary of the Infrared-Band Assignments for Anthracene in Solution

Band (cm <sup>-1</sup> )	Assignment	Additional Information
3048	Aromatic $\nu$ (C–H)	
3021	Aromatic $\nu$ (C–H)	Less intense band different symmetry
3010, 2988 1930–1720	Aromatic $\nu$ (C–H) Overtone or combination bands	Combination bands
1618	$\nu$ (C=C)	
1533	$\nu$ (C=C)	
1488	$\nu$ (C=C)	
1315	$\delta$ (CH) ip	
1272	$\delta$ (CH) ip	
1147	$\delta$ (CH) ip	
883	$\delta$ (CH) oop	Carbon 9 and 10
725	$\delta$ (CH) oop	Carbon 1–4 and 5–8

The presence of product species is apparent after 1 min of ozone addition, evidenced by the formation of broad overlapping bands at 1740, 1693, and 1672 cm<sup>-1</sup>, which are readily assigned to carbonyl species. As ozone exposure continues, a large number of new features are seen to grow in. Many of the new features are readily assigned to generally aromatic moieties, typically aromatic ring modes around 1595, 1480, and 1460 cm<sup>-1</sup>, and strong out-of-plane  $\delta$  (C–H) modes at 753 and 702 cm<sup>-1</sup>. The presence of oxygenated products is suggested by the growth of a number of infrared bands in the O–H stretching region (3590–3120 cm<sup>-1</sup>), O–H bending (1300–1200 cm<sup>-1</sup>), and C–O stretching regions (1110–1030 cm<sup>-1</sup>). Other reasonably easily identified features are the broad bands at ca. 2750 and 2850 cm<sup>-1</sup>, which are characteristic of aldehyde and carboxylic acid species.

The nature of the new species formed upon ozonolysis of anthracene in solution can be obtained from an examination of the resonances in the carbonyl region. Carbonyl  $\nu$ (C=O) frequencies are very sensitive to their local environment, and comparison with group-frequency correlation tables allows the general identification of the presence of aryl ketones (1672 cm<sup>-1</sup>), carboxylic acids (1693 cm<sup>-1</sup>), aldehydes (1710 cm<sup>-1</sup>), esters (1730 cm<sup>-1</sup>), and acid anhydrides (1850 cm<sup>-1</sup>) in the range of products formed. Furthermore, the relative intensities of these individual carbonyl bands is seen to vary significantly as ozone exposure increases, suggesting that different types of products are formed at various stages through the reaction. From the reaction mechanism proposed by Bailey [5], 9,10-anthraquinone is likely to be formed as the major prod-

uct via ozone addition at the carbon atoms situated in the inner ring of anthracene. 9,10-anthraquinone has a characteristic carbonyl band at 1676 cm<sup>-1</sup>, which coincides with the observed band seen in the ozonized samples at 1672 cm<sup>-1</sup>. Upon closer inspection of the spectra of the ozonized samples, some of the other known main bands of 9,10-anthraquinone at 1280, 1212, and 930 cm<sup>-1</sup> can also be identified, although it is not possible to unequivocally identify the  $\delta$ (CH) oop mode, which would be expected around 692 cm<sup>-1</sup>. The species contributing to the acid carbonyl at 1693 cm<sup>-1</sup> are most likely to be compounds containing acid functionality adjacent to a double bond (1715–1680 cm<sup>-1</sup>) or aromatic acids (1700–1680 cm<sup>-1</sup>) such as phthalic acid (1685 cm<sup>-1</sup>), in line with the predictions of Bailey [5]. Although the presence of ester- and aldehyde-type species cannot be explained straightforwardly from the primary mechanism proposed by Bailey [5], their formation can certainly be assumed to be the result of some sort of secondary reactions, because the production of such species is widely documented in a number of comparable ozonized organic systems including as oleic acid [10] and stilbene [16]. At the ozone concentrations used in this study, it is highly likely both that reactions involving oxidation at sites other than the inner-ring positions occur and that further reactions involving ozone addition across remaining unsaturation (either aliphatic or aromatic) in any products are also occurring. The formation of cyclic anhydride species is the most feasible explanation for the band at 1850 cm<sup>-1</sup>, following observations by Gunzler and Gremlich [17], who characterized these species as having symmetric and antisymmetric coupled modes with  $\nu_s$  around 1870–1845 cm<sup>-1</sup> and  $\nu_{as}$  around 1800–1715 cm<sup>-1</sup>.

Toward the end of the reaction, the spectra are strongly redolent of those resulting from the ozonolysis of stilbene in solution, in that they are dominated by broad features characteristic of carbonyl, C–O and OH functionalities, unresolvable and strongly overlapped because of the presence of many similar components. As a result of the complexity of the infrared spectra, the direct identification of reaction products (primary or secondary) cannot therefore be made. However, there are key bands in both the reactant and in some of the products that can be used for kinetic studies and the general nature of the oxidized species formed has been reliably established.

**Mass Spectrometry.** The APCI technique produces both AP<sup>+</sup> and AP<sup>-</sup> spectra. The resulting spectra for anthracene before and after various ozone exposures are shown in Fig. 2. The anthracene starting material

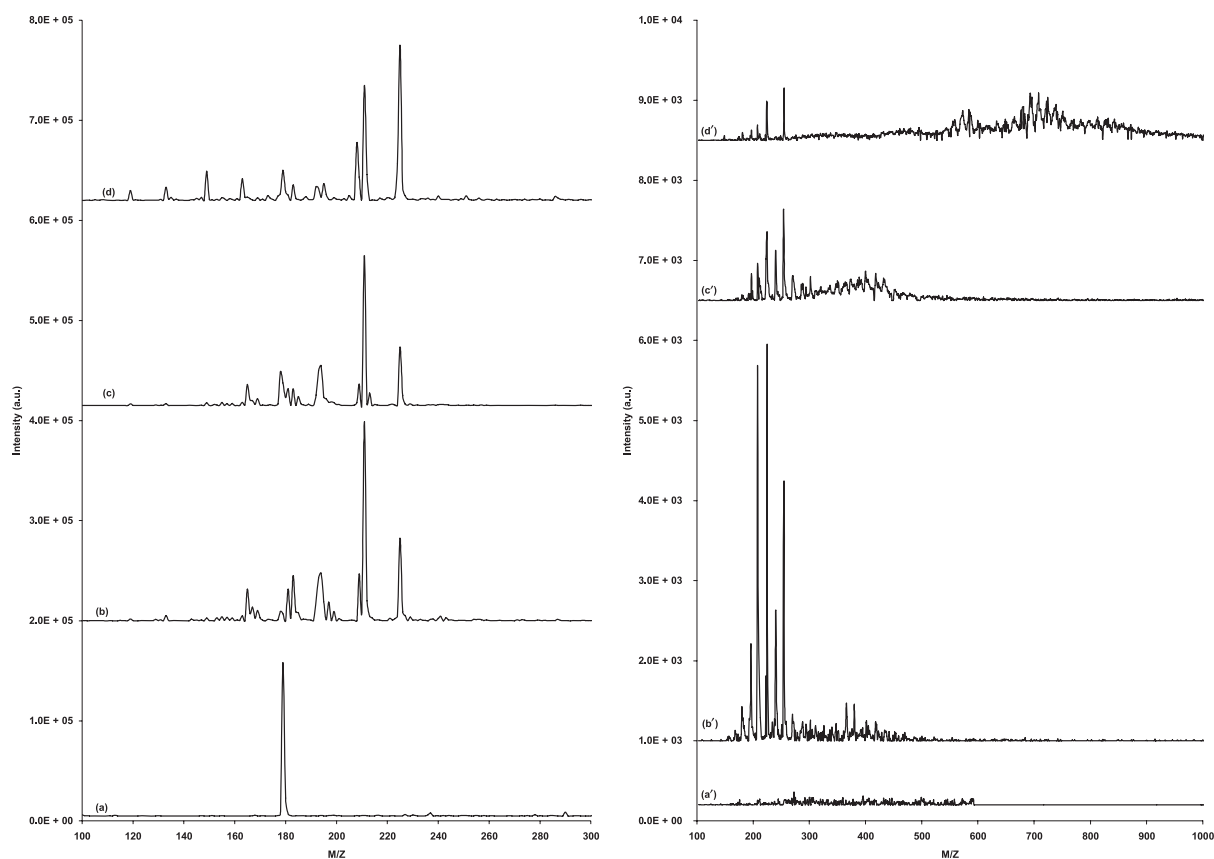


**Figure 2** APCI ( $AP^+$  left and  $AP^-$  right) mass spectra of anthracene exposed to ozone for (a, a') 0 min, (b, b') 1 min, (c, c') 4 min, and (d, d') 8 min.

is seen in the  $AP^+$  spectrum as an intense peak at  $m/z$  179 corresponding to the molecular ion ( $M+H^+$ ). The addition of ozone causes the intensity of the anthracene molecular ion to decrease rapidly (34% loss after 1 min of ozone addition) as products are formed.

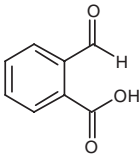
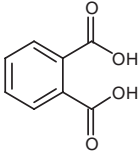
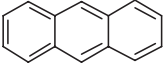
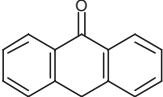
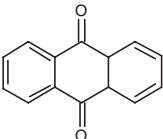
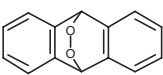
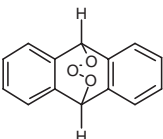
Upon exposure to ozone, a number of additional bands became apparent in the  $AP^+$  mass spectra as a result of product formation. Several suggested oxidation products for the ozonolysis of anthracene are given in Table II. At low ozone exposures, the main product peaks in the  $AP^+$  spectra occur at 226, 209, 194, 193, 183, 181, and 165  $m/z$ , with the most dominant peak at 211  $m/z$ . These peaks suggest that the main product formed is the 9,10-endoperoxide-anthracene, with smaller contributions from 9,10-anthraquinone and dihydroxyanthrones (see Table II). At higher ozone exposures, the initial product peaks are accompanied by new peaks at 224, 212, 208, 163, and 149  $m/z$ .

In contrast to the sparsely populated  $AP^+$  mass spectra, the  $AP^-$  spectra contain an array of peaks for the various ozone exposures. At low ozone expo-

sure, the main peaks can be seen at 255, 241, 207, 195, and 193  $m/z$  with the most dominant peak seen at 225  $m/z$ . Again, this suggests that the main products formed are dihydroxyanthrones, 9,10-endoperoxide-anthracene, 9,10-anthraquinone, and anthrone. At higher ozone exposures, the  $AP^-$  spectra show a significant decrease in the major products ( $m/z$  225, 209, and 207) with a significant increase in the population of peaks at higher mass ions specifically in the region 559–585  $m/z$  and 660–760  $m/z$ . This is most likely due to the formation of oligomers, although direct oligomer speciation is not possible from these data alone. However, the formation of PAH oligomers from ozonolysis is unprecedented and requires further investigation.

The results from these solution-phase experiments therefore allow several products to be identified, which are consistent with the mechanism proposed by Bailey [5]. Evidence in both the infrared and mass spectra strongly suggests the formation of 9,10-anthraquinone, in agreement with a number of other studies in the condensed phase [5], at the air-aqueous interface [8], on surface films [3,6], and on sodium

**Table II** Suggested Structures for Products Responsible for Ions Observed in AP<sup>+</sup> and AP<sup>-</sup> Spectra of Ozonized Anthracene

<i>m/z</i>	Name	Possible Structure
150	2-Formyl-benzoic acid; Bailey [5]	
166	Phthalic acid; Kwamena et al. [8]	
178	Anthracene	
194	Anthrone; Gloaguen et al. [9]	
208	9,10-Anthraquinone; Bailey [5], Gloaguen et al. [9], Mmereki et al. [3], Kwamena et al. [8]	
210	9,10-Endoperoxide—anthracene; Gloaguen et al. [9]	
226	Dihydroxyanthrones	

chloride particles [9]. It has previously been proposed that 9,10-anthraquinone can either be formed directly by ozone addition at the two inner-ring carbon atoms of anthracene or indirectly by decomposition of a hydroperoxide intermediate [5]. In this study, the mass spectra contain strong evidence for the formation of dihydroxyanthrones species, which have previously been detected by Gloaguen et al. in experiments utilizing vacuum ultraviolet aerosol mass spectrometry [9]. Many of the lower intensity peaks in the solution mass spectra can potentially be attributed to the formation of phthalic acid (at 165 *m/z*) and anthrone (at 194 *m/z*), species, which have been detected in previous studies [5,8,9]. In the reaction mechanism proposed by Bailey, anthrone is an intermediate that subsequently forms 9,10-anthraquinone [5]. This mechanism and previous studies can account for a substantial proportion of the products formed in the solution-phase experiments but

does not provide a route to the formation of higher mass species, which arise from secondary reactions and/or oligomer fragments. As noted earlier, the formation of oligomers occurs mainly in bulk solution [10,18] and thus does not reflect physical mass transport of material in interfacial regions associated with gas-phase and condensed-phase processes.

The relatively crude APCI method used in these studies produces a significant amount of fragmentation, and the spectra thus obtained are not amenable to a more sophisticated analysis of the nature of oligomeric products. Indeed, direct observation and characterization of the oligomers formed in oleic acid ozonolysis in previous studies has only been effective through the use of ion-trap mass spectrometry with sufficient sensitivity and selectivity separate and structurally characterize the high-molecular-weight species [18].

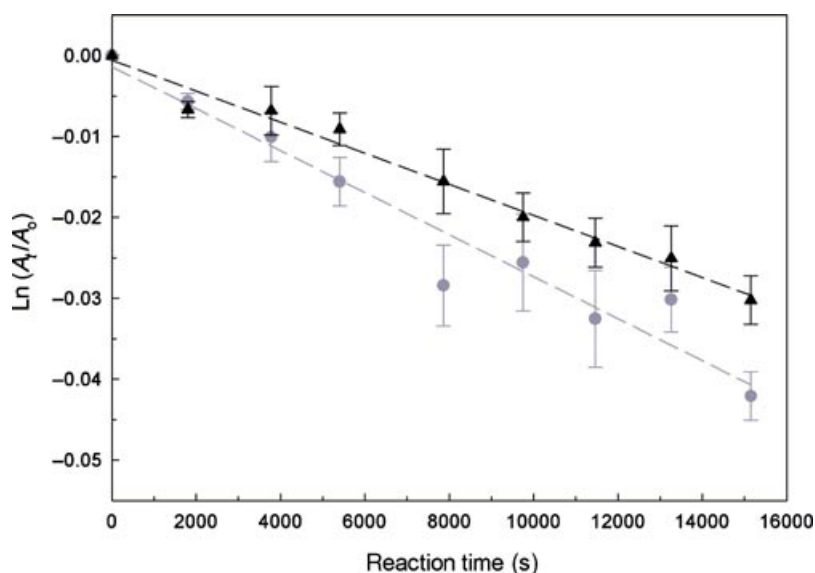


**Figure 3** Decay of anthracene  $\nu$  (C–H) (gray circle) and  $\delta$  (C–H) (black triangle) bands under exposure to 2 ppm ozone over the course of 4.5 h. The error bars are derived from the mean of three spectra. [Color figure can be viewed in the online issue, which is available at [wileyonlinelibrary.com](http://wileyonlinelibrary.com).]

### Kinetics of the Ozonolysis Reaction in a Thin Film

From the solution-phase reaction studies, two infrared bands suitable for monitoring the kinetics of anthracene loss upon ozonolysis were identified, namely the  $\nu$  (C–H) band at  $3050\text{ cm}^{-1}$  and one of the  $\delta$  (C–H)-oop bands at  $883\text{ cm}^{-1}$ . For quantification purposes, the  $\nu$  (C–H) band was integrated between  $3070$  and  $3032\text{ cm}^{-1}$ , and the  $\delta$  (C–H) band between  $897$  and  $866\text{ cm}^{-1}$ . Kinetic studies were performed under pseudo-first-order conditions with ozone as the excess reagent (using ozone concentrations of  $5 \times 10^{13}$  molecules  $\text{cm}^{-3}$  with a corresponding total anthracene concentration of  $1.4 \times 10^{12}$  molecules  $\text{cm}^{-3}$  in the cast film). (Note that this is a rather crude estimate, because the majority of the anthracene molecules present are located within the bulk of the thin film, making them inaccessible to the incoming ozone. As a result, the actual excess of ozone molecules over anthracene molecules in the reaction zone is likely to be several orders of magnitude greater than this ratio.) For any given anthracene band, the reactant loss can be determined using

$$\ln \frac{A_t}{A_0} = -k'_1 t \quad (1)$$

where  $A_0$  is the initial absorbance determined as the anthracene-integrated band area before the addition of ozone,  $A_t$  is the absorbance at a given time  $t$ , and

$k'_1$  is the pseudo-first-order rate constant. A plot of  $\ln (A_t/A_0)$  versus  $t$  for this reaction will therefore yield a straight line with the gradient equal to the pseudo-first-order rate constant. The logarithmic decay for the integrated  $\nu$  (C–H) and  $\delta$  (C–H) bands of anthracene is shown in Fig. 3. The error bars are derived from the mean of three experiments. Quantitative agreement was observed by both methods, although the  $\delta$  (C–H) band is preferred, as the signal-to-noise ratio is higher and consequently less scatter in the data points. The value of the pseudo-first-order constant,  $k'_1$ , for the ozonolysis of anthracene after correction for wall losses, was determined as  $(2.5 \pm 1.3) \times 10^{-6}\text{ s}^{-1}$ .

As observed in other studies [11,16], a reactive uptake coefficient ( $\gamma$ ) can be calculated assuming that the ozonolysis reaction takes place only at the surface by

$$\gamma = \frac{4RT}{\bar{c}} \frac{V}{S_A} \frac{k'_1}{P_{O_3}} [\text{Anthracene}] \quad (2)$$

where  $T$  is the temperature (298 K),  $\bar{c}$  is the mean molecular speed of ozone ( $360\text{ m s}^{-1}$ ),  $V$  is the volume of the film,  $S_A$  is the surface area of the film (the ratio  $V/S_A$  is the film thickness, i.e.,  $75\text{ nm}$ ),  $P_{O_3}$  is the partial pressure of ozone ( $1.8 \times 10^{-6}\text{ atm}$ ), and  $[\text{Anthracene}]$  is the concentration of anthracene ( $7.01\text{ mol L}^{-1}$ ) based on the density and molecular weight. The surface reactive uptake for anthracene was thus determined to be  $(2.0 \pm 1.1) \times 10^{-7}$ .



## Kinetic Studies of the Ozonolysis Reaction of Anthracene Aerosols

**Characterization of Anthracene-Coated  $(\text{NH}_4)_2\text{SO}_4$  Particles.** The vapor pressure of anthracene below 200°C is insufficient to form aerosols through homogeneous nucleation [11], and so a heterogeneous method in which an  $(\text{NH}_4)_2\text{SO}_4$  seed is used as a nucleation substrate was adopted [16]. Once coated, the aerosol particles were then characterized using a TOPAS particle-size analyzer before entering the AFT. Typically, the mean particle diameter for the seed particles was 0.7  $\mu\text{m}$ . When coated, the particle diameter increases to 0.9  $\mu\text{m}$ ; hence the particles are coated with a 0.2- $\mu\text{m}$  shell of anthracene. The number density of coated particles was typically  $11.0 \times 10^5$  particles  $\text{cm}^{-3}$ . The particles are diluted on entering the AFT by the additional sheath flow, giving a particle number density within the AFT of  $3.2 \times 10^5$  particles  $\text{cm}^{-3}$ , which equates to an anthracene concentration of  $1.2 \times 10^{13}$  molecules  $\text{cm}^{-3}$ .

Representative infrared spectra of the  $(\text{NH}_4)_2\text{SO}_4$  seed, coated particle, and ozonized coated particle are shown in Fig. 4. The  $(\text{NH}_4)_2\text{SO}_4$  aerosol spectrum is characterized by the  $\nu$  ( $\text{NH}_4^+$ ) mode between 3350 and 2650  $\text{cm}^{-1}$ , the  $\delta$  ( $\text{NH}_4^+$ ) mode between 1470 and 1395  $\text{cm}^{-1}$ , the  $\nu$  ( $\text{SO}_4^{2-}$ ) mode between 1180 and 1050  $\text{cm}^{-1}$ , and the weak  $\delta$  ( $\text{SO}_4^{2-}$ ) mode between 634 and 605  $\text{cm}^{-1}$ . When coated, the main characteristic bands of anthracene are seen superimposed on the  $(\text{NH}_4)_2\text{SO}_4$  spectrum. Although ozonolysis at short contact times with low ozone concentrations results in the formation of only a small amount of product, some new weak features are nevertheless discernible in the oxidized aerosols. The most obvious new band is the carbonyl stretch at around 1700  $\text{cm}^{-1}$ , just discernible above the noise. Another significant feature is seen at approximately 690  $\text{cm}^{-1}$ , most likely due to a  $\delta$  (CH) oop mode of one of the products. The  $\nu$  (C–H) mode of anthracene is not very distinct in these dilute conditions and hence the kinetics of the ozonolysis reaction can only be followed via the  $\delta$  (C–H) band. For quantification purposes, this band was integrated between 893 and 872  $\text{cm}^{-1}$  and normalized to the integrated intensity of the  $\delta$  ( $\text{NH}_4^+$ ) band of the seed species [16].

**Kinetics of the Ozonolysis Reaction of Anthracene Aerosols.** Kinetic studies were performed under pseudo-first-order conditions with ozone as the excess reagent, with ozone concentrations in the range of  $0.4\text{--}1.8 \times 10^{16}$  molecules  $\text{cm}^{-3}$  (as compared with

the anthracene concentration of  $1.2 \times 10^{13}$  molecules  $\text{cm}^{-3}$  in the particle phase). As for the thin-film studies, a plot of  $\ln(A_t/A_0)$  versus time yielded a straight line with the gradient equal to the observed rate constant, in this case denoted as  $k_{\text{obs}}$ . The errors associated with  $k_{\text{obs}}$  were obtained to the  $1\sigma$  level from the linear regression of the plots. The values of  $k_{\text{obs}}$  obtained from the anthracene–aerosol experimental data as a function of ozone concentration are shown in Fig. 5.

Although the scatter in the data is quite large (and could feasibly be fitted by a straight line, although such a line would not intercept the origin), the data were fitted on the basis of a Langmuir–Hinshelwood-type mechanism for comparison with other similar experimental studies [2,19,20]. This mechanism is based upon the simple premise that the reaction occurs on the surface between two adsorbed reactants. In this case, one reactant is permanently adsorbed (anthracene) and the surface concentration of the second reactant (ozone) is determined by an adsorption/desorption equilibrium (based loosely on the Langmuir adsorption isotherm). The parameters that describe the Langmuir–Hinshelwood mechanism are the partitioning coefficient for ozone onto the aerosol surface ( $K_{\text{O}_3}$ ) and the maximum pseudo-first-order rate coefficient for the surface reaction between anthracene and adsorbed ozone ( $k_{\text{max}}^1$ ) [19,21,22]. As the ozone concentration in the gas phase increases, the number of surface sites available for ozone adsorption becomes saturated, which allows a maximum reaction rate to be observed. The experimentally observed reaction rate coefficient,  $k_{\text{obs}}$ , is related to these parameters as follows [21,22]:

$$k_{\text{obs}} = \frac{k_{\text{max}}^1 K_{\text{O}_3} [\text{O}_3(\text{g})]}{1 + K_{\text{O}_3} [\text{O}_3(\text{g})]} \quad (3)$$

where  $[\text{O}_3(\text{g})]$  is the concentration of ozone. The values of  $k_{\text{max}}^1$  and  $K_{\text{O}_3}$  can be determined using a non-linear least-squares fit of Eq. (3) (using a rectangular hyperbola function) to the experimental  $k_{\text{obs}}$  data as a function of the ozone concentration. For the data in Fig. 5,  $k_{\text{max}}^1$  was found to be  $0.035 \pm 0.016 \text{ s}^{-1}$  and  $K_{\text{O}_3}$  to be  $(1.4 \pm 1.7) \times 10^{-16} \text{ cm}^3 \text{ molecules}^{-1}$  as shown in Table III, where the reported errors are at the  $1\sigma$  level. Table III also summarizes the literature values for heterogeneous ozonolysis of anthracene on different aerosol substrates. On the assumption of a Langmuir–Hinshelwood reaction mechanism, the  $[\text{O}_3]$ -dependent reactive uptake coefficient,  $\gamma$ , for anthracene-coated  $(\text{NH}_4)_2\text{SO}_4$  aerosols can also be obtained from this

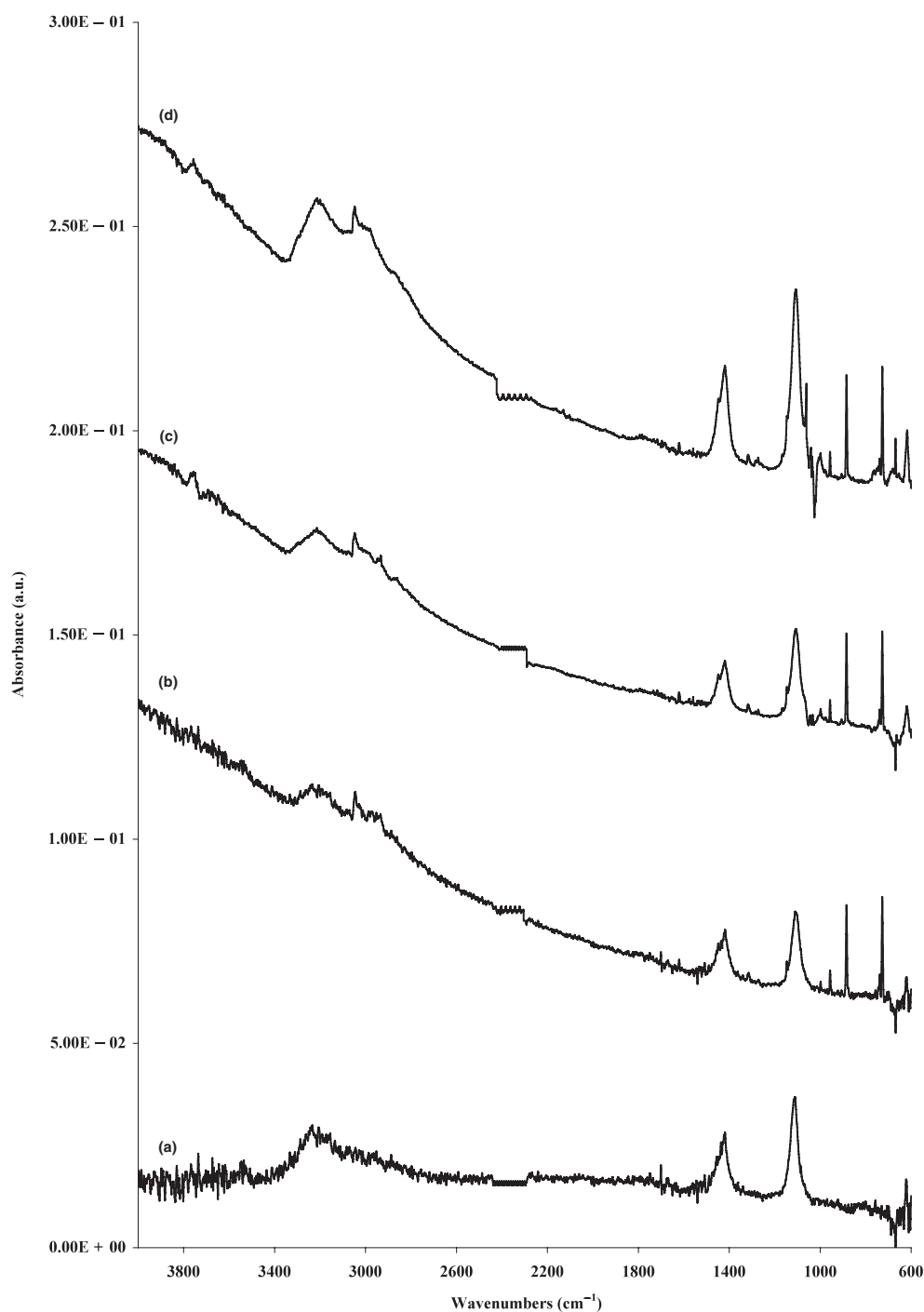


**Figure 4** AFT-FTIR spectra of aerosol particles: (a)  $(\text{NH}_4)_2\text{SO}_4$  seed, (b) anthracene-coated seed, (c) initial ozone addition, and (d) final ozone addition.

data using Eq. (4) if the ozone concentration is known.

$$\gamma = \frac{4k_{\max}^I K_{\text{O}_3}}{\sigma_{\text{org}} C_{\text{O}_3} (1 + K_{\text{O}_3} [\text{O}_3])} \quad (4)$$

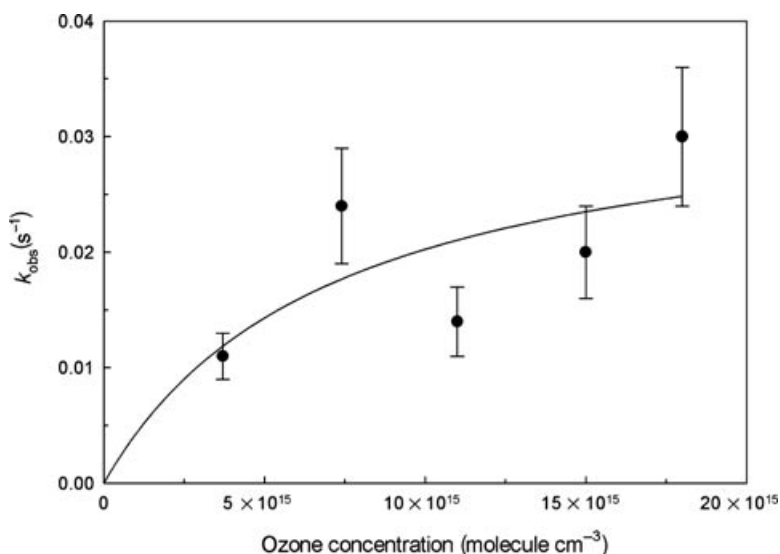
where the terms have their previously described meanings.

## Discussion

From the above results, it is therefore clear that the ozonolysis of anthracene produces a wide range of products that can be detected by infrared spectroscopy and mass spectrometry, although quantitation and direct speciation of these products is challenging. There

**Table III** Comparison of Langmuir–Hinshelwood Parameters Obtained for the Heterogeneous Reaction of Ozone with Anthracene on Aerosol Seeds

	$\sigma$ Molecule ( $\text{cm}^{-2}$ )	Aerosol Seed	$k_{\text{max}}^I$ ( $\text{s}^{-1}$ )	$K_{\text{O}_3}$ ( $\text{cm}^3 \text{ molecule}^{-1}$ )	$D_p/(\text{nm})$ (Seed)	$\gamma$
Kwamena [2]	$3.33 \times 10^{-14}$	Phenylsiloxane oil	$0.010 \pm 0.003$	$(1.0 \pm 0.4) \times 10^{-13}$	175	$(1.4-0.2) \times 10^{-6}$
Kwamena [2]	$3.33 \times 10^{-14}$	Azelaic acid	$0.057 \pm 0.009$	$(2.2 \pm 0.9) \times 10^{-15}$	145	$(3.8-2.0) \times 10^{-7}$
This work	$5.9 \times 10^{-15}$	Ammonium sulfate	$0.035 \pm 0.016$	$(1.4 \pm 1.7) \times 10^{-16}$	600	$(5.6-3.1) \times 10^{-8}$

**Figure 5** Pseudo-first-order reaction rate constant for anthracene coating on  $(\text{NH}_4)_2\text{SO}_4$  aerosol particles as a function of the ozone concentration. The solid line shows a fit of the data to the Langmuir–Hinshelwood mechanism using nonlinear least-squares fit of Eq. (3) based on a rectangular hyperbola function.

seems to be little variation in product distribution between solution, aerosols, and thin films as far as can be identified from these experiments. The main feature of the results comes from an analysis of kinetic trends. The kinetics of ozone uptake on thin films of anthracene on a variety of substrates has been measured previously in a number of studies. Figure 6 shows a summary of all currently available experimental data for reactive uptake coefficients from both thin films and aerosols. Uptake coefficients ranging between  $(6.6-0.7) \times 10^{-8}$  and  $(23-0.7) \times 10^{-8}$  have been obtained for air–organic (octanol and decanol) [7] and air–aqueous (uncoated water, 1-octanol, hexanoic, octanoic and stearic acid) interfaces [3], respectively, and an uptake coefficient of  $(6.2-0.5) \times 10^{-8}$  has been reported for anthracene adsorbed on Pyrex tubes [8]. All studies show a significant dependence

of the uptake coefficient on the ozone concentration, again likely to be the result of ozone partitioning. There is a notable increase in the experimentally determined  $\gamma$  values as the ozone concentration decreases. The ozonolysis of anthracene is significantly slower than that obtained from the ozonolysis reaction of other PAH systems, such as benzo(a)pyrene. Aerosol experiments of benzo(a)pyrene coated on azelaic acid and soot particles determined reactive uptakes of  $5 \times 10^{-7}$  and  $2 \times 10^{-5}$ , respectively [19,20]. The reactive uptake of ozone onto anthracene is also significantly slower in comparison with other organic compounds cast onto IRE crystals (cf. oleic acid  $7.5 \times 10^{-5}$  [11] and stilbene  $7.8 \times 10^{-5}$  [16]), although this is hardly surprising, given that they contain accessible olefinic C=C bonds.

As can be seen from Fig. 6, there appears to be a significant variation (by a factor of around 5–10) between

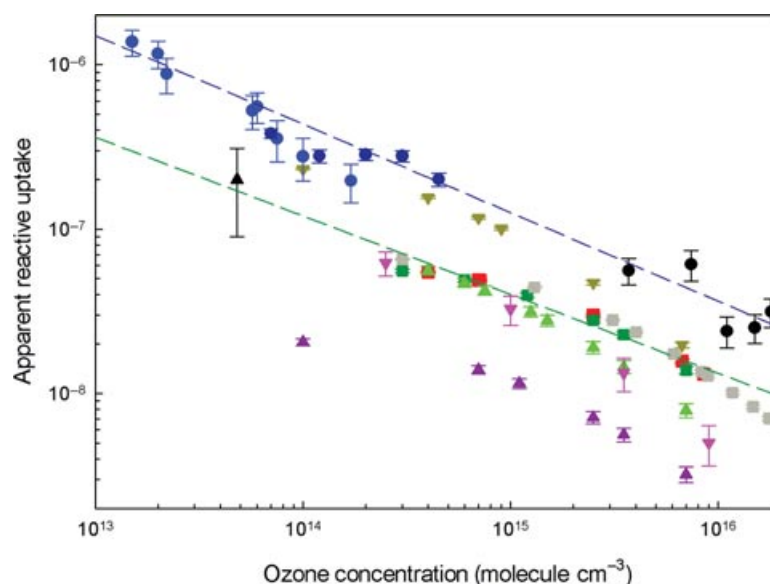


**Figure 6** Summary of the apparent reactive uptake for the ozonolysis reaction of anthracene on different surface substrates. The  $\gamma$  values determined here for anthracene on ZnSe and  $(\text{NH}_4)_2\text{SO}_4$  aerosols are shown as black triangles and black circles, respectively. The  $\gamma$  values were adapted from Mmereki and Donaldson [6] (red squares for water and dark yellow triangles for 1-octanol), Mmereki et al. [3] (dark-green squares for stearic acid, green triangles for octanoic acid and purple triangles for hexanoic acid), Kahan et al. [7] (gray squares for octanol/decanol), Kwamena et al. [8] (pink triangles for Pyrex), and Kwamena et al. [2] (blue circles for phenylsiloxane oil aerosols and dark-blue circles for azelaic acid aerosols). See Tables III and IV for details. [Color figure can be viewed in the online issue, which is available at [wileyonlinelibrary.com](http://wileyonlinelibrary.com).]

the trends in thin-film and aerosol kinetic data. For the reaction of a thin film of anthracene on a ZnSe surface reported here, the  $\gamma$  value obtained at lower ozone concentrations is somewhat smaller at  $(2.0 \pm 1.1) \times 10^{-7}$  than those for anthracene on phenylsiloxane aerosols at comparable  $[\text{O}_3]$  [2], but lies firmly on an extrapolation (green dashed line) of other thin-film measurements made at higher  $[\text{O}_3]$ . The  $\gamma$ -coefficients for the reaction of anthracene on  $(\text{NH}_4)_2\text{SO}_4$  aerosols are also plotted in Fig. 6, decreasing from  $5.6 \times 10^{-8}$  to  $3.1 \times 10^{-8}$  as the ozone concentration increases. Although these values lie considerably above those obtained by Mmereki et al. for stearic, octanoic, and hexanoic acids and octanol at aqueous interfaces in this  $[\text{O}_3]$  range [3], they lie directly along an extrapolation (blue dashed line) of data from anhydrous experiments by Kwamena et al. at lower  $[\text{O}_3]$  [2]. Supporting this observation, direct comparison of the aerosol Langmuir–Hinshelwood parameters with those from other studies (summarized in Tables III and IV) shows that the  $k_{\text{max}}^{\text{I}}$  values for anthracene on  $(\text{NH}_4)_2\text{SO}_4$  aerosols lie directly between those for anthracene adsorbed on phenylsiloxane oil and azelaic acid aerosols, which are, in comparison, about an order of magnitude higher than those for anthracene at aqueous (organic) interfaces and on Pyrex.

No such order exists between the tabulated  $K_{\text{O}_3}$  values; however, the value obtained for  $(\text{NH}_4)_2\text{SO}_4$  aerosols is one order of magnitude lower than for azelaic acid and three orders of magnitude lower than for phenylsiloxane oil aerosols. Kwamena et al. [2] previously suggested that for various PAHs on different aerosol substrates, the values of  $k_{\text{max}}^{\text{I}}$  would be similar whereas the partitioning of ozone, i.e.,  $K_{\text{O}_3}$ , would vary significantly depending on the substrate used. The results from this study support this latter notion, in that the  $K_{\text{O}_3}$  values cover a wide range. The most plausible explanation for the rather small value of  $K_{\text{O}_3}$  for  $(\text{NH}_4)_2\text{SO}_4$  particles is high surface polarity, given that it is well known that gas-phase ozone will partition efficiently to nonpolar substrates. The ionic nature of  $(\text{NH}_4)_2\text{SO}_4$  aerosol and the likely presence of strongly adsorbed water give it a low affinity for ozone, comparable to that of aqueous interfaces. It seems likely, however, that there are other, larger factors that affect  $k_{\text{max}}^{\text{I}}$  values, including surface geometry (flat surface versus curved aerosol) and adsorbate morphology (monolayers versus multilayers/islands). This trend has also been observed for oleic acid, in that rate constants obtained on thin films are generally smaller than those obtained from aerosols [11].

**Table IV** Comparison of Langmuir–Hinshelwood Parameters Obtained for the Heterogeneous Reaction of Ozone with Anthracene on Different Substrates and Aerosol Seeds

	$O_3$ (molecule $cm^{-3}$ )	$\sigma$ (molecule $cm^{-2}$ )	Aerosol Seed or Substrate	$k_{max}^I$ ( $s^{-1}$ )	$K_{O_3}$ ( $cm^3$ molecule $^{-1}$ )	$\gamma$
Mmereki [6]	$(0.4-8.5) \times 10^{15}$	$2.03 \times 10^{-15}$	Water	$(2.55 \pm 0.17) \times 10^{-3}$	$(4.66 \pm 0.59) \times 10^{-16}$	$(5.4-1.3) \times 10^{-8}$
Mmereki [6]	$(0.1-6.7) \times 10^{14}$	$2.03 \times 10^{-15}$	1-octanol aq.	$(2.59 \pm 0.14) \times 10^{-3}$	$(1.96 \pm 0.34) \times 10^{-15}$	$(2.3-0.2) \times 10^{-7}$
Mmereki [3]	$(0.3-7.0) \times 10^{15}$	$2.03 \times 10^{-15}$	Stearic acid aq. film	$(2.26 \pm 0.20) \times 10^{-3}$	$(5.2 \pm 1.3) \times 10^{-16}$	$(5.6-1.4) \times 10^{-8}$
Mmereki [3]	$(0.4-7.0) \times 10^{14}$	$2.03 \times 10^{-15}$	Octanoic acid aq.	$(1.11 \pm 0.12) \times 10^{-3}$	$(1.46 \pm 0.62) \times 10^{-15}$	$(5.6-0.8) \times 10^{-8}$
Mmereki [3]	$(0.1-7.0) \times 10^{14}$	$2.03 \times 10^{-15}$	Hexanoic acid aq.	$(0.48 \pm 0.07) \times 10^{-3}$	$(8.47 \pm 2.56) \times 10^{-16}$	$(2.0-0.3) \times 10^{-8}$
Kahan [7]	$(0.03-1.8) \times 10^{16}$	$2.03 \times 10^{-15}$	Octanol and decanol	$(2.5 \pm 0.1) \times 10^{-3}$	$(5.6 \pm 1.2) \times 10^{-16}$	$(6.6-0.7) \times 10^{-8}$
Kwamena [8]	$(0.2-9.0) \times 10^{15}$	$1.43 \times 10^{-14}$	Pyrex glass	$(6.4 \pm 1.8) \times 10^{-3}$	$(2.8 \pm 0.9) \times 10^{-15}$	$(6.2-0.5) \times 10^{-8}$
Kwamena [2]	$(0.1-1.7) \times 10^{14}$	$3.33 \times 10^{-14}$	Phenylsiloxane oil	$0.010 \pm 0.003$	$(1.0 \pm 0.4) \times 10^{-13}$	$(1.4-0.2) \times 10^{-6}$
Kwamena [2]	$(0.1-4.5) \times 10^{14}$	$3.33 \times 10^{-14}$	Azelaic acid	$0.057 \pm 0.009$	$(2.2 \pm 0.9) \times 10^{-15}$	$(3.8-2.0) \times 10^{-7}$
This work	$(0.4-1.8) \times 10^{16}$	$5.9 \times 10^{-15}$	Ammonium sulfate	$0.035 \pm 0.016$	$(1.4 \pm 1.7) \times 10^{-16}$	$(5.6-3.1) \times 10^{-8}$
This work	$5 \times 10^{13}$		Zn Se	—	—	$(2.0 \pm 1.1) \times 10^{-7}$

## CONCLUSIONS

In this study, a number of the products formed during the ozonolysis reaction of anthracene in the bulk phase were identified by infrared spectroscopy and APCI mass spectrometry. These results reveal the formation of a diverse array of species with various oxygenated functionality, including aldehydes, aryl ketones, esters, acids, and anhydrides (which are most likely cyclic in nature). The main identifiable ozonolysis products were anthrone, phthalic acid, 9,10-anthraquinone, 9,10-endoperoxide—anthracene, and dihydroxyanthrones, in good agreement with other studies of anthracene ozonolysis [8,9,23]. The mass spectrometric results at longer ozone exposure times show strong evidence for substantial anthracene-ring opening. Such reactions could lead to the formation of secondary products and oligomers, for which there is also evidence in the mass spectra. Existing mechanisms for anthracene reported in the literature [5] cannot account for either the high-molecular-mass species or the formation of ester and aldehyde functional compounds. To determine the exact structure of the larger molecular weight products and further develop the anthracene reaction mechanism, other more structurally resolved analytical techniques (such as ion-trap mass spectrometry, previously used for oleic acid oligomer characterization [18]) are required.

The ATR-IR method utilized in the thin-film experiments enabled the anthracene loss to be monitored directly via the  $\delta$  (C–H) band, thus allowing for a pseudo-first-order rate constant to be determined. A reactive uptake coefficient of  $(2.0 \pm 1.1) \times 10^{-7}$  was obtained for anthracene ozonolysis assuming a surface reaction. This is significantly slower than that for oleic acid [11] and *cis*-stilbene [16] ozonolysis measured in the same experimental system and also for several other PAH system investigated in thin films [19,20,24]. However, the value obtained in this study is in good agreement with values reported in the literature for anthracene on various other aerosol substrates [3, 6–8].

Direct measurements of the reactive uptake coefficient for anthracene films on  $(NH_4)_2SO_4$  aerosols obtained by infrared spectroscopy produced values in the range  $5.6 \times 10^{-8}$  to  $3.1 \times 10^{-8}$ . The data obtained as a function of the ozone concentration give a pseudo-first-order maximum surface rate constant,  $k_{max}^I$ , of  $3.5 \times 10^{-2}$  and an ozone partition coefficient,  $K_{O_3}$ , of  $1.4 \times 10^{-16}$ . Comparison of these values with literature data on other substrates reveals that the principal factor affecting the rate is the ozone partitioning, which is known to be affected by the polarity of the substrate [2,25].

A comparison of the reactive uptake coefficients for ozone on a wide range of substrates as a function of the ozone concentration shows a pronounced trend, with the majority of experimental data (including that reported in this paper) falling onto one of two trend lines on a log–log plot of  $\gamma$  versus  $[O_3]$ . In general, rate constants and uptake coefficients from measurements on aerosols are found to be 5–10 times faster than those measured on thin films. Reasons for this behavior are far from obvious, but could include the effect of surface curvature, adsorbate morphology, and/or the ability of ozone to penetrate or diffuse within the reactant layer. Further experiments are needed to resolve this issue.

RW and KEL thank Natural Environment Research Council (NERC) for doctoral studentships. CJP and ABH thank NERC and the Leverhulme Trust, under whose auspices various parts of this work were carried out.

## BIBLIOGRAPHY

1. Finlayson-Pitts, B. J.; Finlayson-Pitts, P. J. N. *Chemistry of the Upper and Lower Atmosphere. Theory, Experiments and Applications*; Academic Press: New York, 2000.
2. Kwamena, N. O. A.; Staikova, M. G.; Donaldson, D. J.; George, I. J.; Abbatt, J. P. D. *J Phys Chem A* 2007, 111, 11050–11058.
3. Mmereki, B. T.; Donaldson, D. J.; Gilman, J. B.; Eliason, T. L.; Vaida, V. *Atmos Environ* 2004, 38, 6091–6103.
4. Pitts, J. N., Jr.; Van Cauwenberghe, K. A.; Grosjean, D.; Schmid, J. P.; Fitz, D. R.; Belser, W. L.; Knudson, G. P.; Hynds, P. M. *Science* 1978, 202, 515–519.
5. Bailey, P. S. *Ozonation in Organic Chemistry*; Academic Press: New York, 1982.
6. Mmereki, B. T.; Donaldson, D. J. *J Phys Chem A* 2003, 107, 11038–11042.
7. Kahan, T. F.; Kwamena, N.-O. A.; Donaldson D. J. *Atmos Environ* 2006, 40, 3448–3459.
8. Kwamena, N.-O. A.; Earp, M. E.; Young, C. J.; Abbatt, J. P. D. *J Phys Chem A* 2006, 110, 3638–3646.
9. Gloaguen, E.; Mysak, E. R.; Leone, S. R.; Ahmed, M.; Wilson, K. R. *Int J Mass Spectrom* 2006, 258, 74–85.
10. Last, D. J.; Najera, J. J.; Wamsley, R.; Hilton, G.; McGillen, M.R.; Percival, C. J.; Horn, A. B. *Phys Chem Chem Phys* 2009, 11, 1427–1440.
11. Last, D. J.; Najera, J. J.; Percival, C. J.; Horn, A. B. *Phys Chem Chem Phys* 2009, 11, 8214–8225.
12. Sander, S. P.; Friedl, R. R.; Ravishankara, A. R.; Golden, D. M.; Kolb, C. E.; Kurylo, M. J.; Molina, M. J.; Moortgat, G. K.; Keller-Rudek, H.; Finlayson-Pitts, B. J.; Wine, P. H.; Huie R. E.; Orkin, V. L. *Chemical Kinetics and Photochemical Data for Use in Atmospheric Studies: Evaluation Number 15*; JPL Publication, 2006.
13. Najera, J. J.; Fochesatto, J. G.; Last, D. J.; Percival, C. J.; Horn A. B. *Rev Sci Instrum* 2008, 79, 124102.
14. Bree, A.; Kydd, R. A. *J Chem Phys* 1968, 48, 5319–5325.
15. Madhurambal, G.; Srinivasan, P. A. *Cryst Res Technol* 2006, 41, 231–235.
16. Wamsley, R. *Studies of Heterogeneous Transformation of Atmospheric Particles*, PhD thesis, University of Manchester, Manchester, UK, 2010.
17. Gunzler, H.; Gremlich, H.-U. *IR Spectroscopy: An Introduction*; Wiley-VCH: Weinheim, Germany, 2002.
18. Reynolds, J. C.; Last, D. J.; McGillen, M.; Nijs, A.; Horn, A. B.; Percival, C.; Carpenter, L. J.; Lewis, A. C. *Environ Sci Technol* 2006, 40, 6674–6681.
19. Poeschl, U.; Letzel, T.; Schauer, C.; Niessner, R. *J Phys Chem A* 2001, 105, 4029–4041.
20. Kwamena, N.-O. A.; Thornton, J. A.; Abbatt, J. P. D. *J Phys Chem A* 2004, 108, 11626–11634.
21. Ammann, M.; Poeschl, U.; Rudich, Y. *Phys Chem Chem Phys* 2003, 5, 351–356.
22. Poeschl, U.; Rudich Y.; Ammann, M. *Atmos Chem Phys* 2007, 7, 5989–6023.
23. Perraudin, E.; Budzinski, H.; Villenave, E. *Atmos Environ* 2007, 41, 6005–6017.
24. Segal-Rosenheimer, M.; Dubowski, Y. *J Phys Chem C* 2007, 111, 11682–11691.
25. Vieceli, J.; Ma, O. L.; Tobias, D. J. *J Phys Chem A* 2004, 108, 5806–5814.